arXiv:1512.09085v1 [astro-ph.IM] 30 Dec 2015

SOLVEPOL: a reduction pipeline for imaging polarimetry data

Edgar A. Ramírez
Inst. de Astronomia, Geofísica e Ciências Atmosféricas, Universidade de São Paulo, SP 05508-900, Brazil.
e.ramirez@usp.br

Antônio M. Magalhães
Inst. de Astronomia, Geofísica e Ciências Atmosféricas, Universidade de São Paulo, SP 05508-900, Brazil.

James W. Davidson Jr.
Astronomy Department, University of Virginia, 530 McCormick Rd. Charlottesville, VA 22904-4325, USA.

Antonio Pereyra
Instituto Geofísico del Perú, Área Astronomía, Calle Badajoz 169, Lima, Perú.
and

Marcelo Rubinho
Inst. de Astronomia, Geofísica e Ciências Atmosféricas, Universidade de São Paulo, SP 05508-900, Brazil.

ABSTRACT

We present a newly pipeline to analyse polarimetric data: SOLVEPOL. This pipeline is based on existing routines previously developed by our polarimetry group at Instituto de Astronomía, Geofísica e Ciências Atmosféricas (IAG) of the University of São Paulo (USP). SOLVEPOL is completely automatic, speeding up the data reduction time, and is capable of handling large data sets. SOLVEPOL is written in INTERACTIVE DATA LANGUAGE (IDL). We present pilot analyses on various optical polarimetric fields that have been previously reduced with our other existing routines, and show that the results from SOLVEPOL are consistent with those reported in the literature. The present pipeline is the basis to develop a reduction pipeline for the optical polarimetric survey SOUTH POL.

Subject headings: Physical data and processes: polarization. Interstellar Medium (ISM), Nebulae: ISM: general. Astronomical Instrumentation, Methods and Techniques: techniques: image processing.

1. Introduction

The observational basis for astrophysics has been generally developed by measuring the radiation flux or brightness of objects, either in broadband or in spectral form, regardless of the polarization state of the light beam.

There are several processes however that polarize (linearly or circularly) the incoming light beam, either at the source or along the way to the observer. Therefore we stand to gain a lot of information, encoded in the polarization state of light, by measuring such polarization. Examples of such processes in ultra-violet (UV)/optical/near-infrared (NIR) domain, and places they might appear, are:

- Dust scattering: Interstellar Medium (ISM); Envelopes of Young Stellar Objects; En-

velopes around asymptotic giant branch (AGB) stars.

- Thomson scattering: Cosmic Microwave Background (CMB); Envelopes of hot stars.
- Synchrotron radiation: Active Galactic Nuclei (AGN) and AGN hot spots; Gamma-ray Bursts (GRBs).
- Cyclotron radiation: Magnetic cataclysmic binaries (polars).

Despite the increase in the use of optical/NIR imaging polarimetry and spectropolarimetry in the past few decades (eg., Trujillo-Bueno et al. 2002; Adamson et al. 2005; Bastien et al. 2011), and in contrast with the radio/sub-mm domain, large area polarimetric surveys are few. Efforts towards improving this have led to several surveys in the past few years. GPIPS, a NIR Galactic Plane Infrared Polarization Survey (Clemens et al. 2012), is a notable one. Another example is the Southern Interstellar Polarization survey (Magalhães et al. 2005), aimed at obtaining optical polarization towards selected areas of (mostly) the Galaxy, in and out of the Plane. SOUTH POL (Magalhães et al. 2012), a broad band, all-sky polarimetric survey in the optical is slated to begin in late 2015.

Surveys and/or large area programs, by their nature, typically need to have some form of data reduction pipeline. A 2k×2k charge-coupled device (CCD) on a moderate, meter-sized telescope might provide several hundred polarized stars from a $\sim 10' \times 10'$ field. The need to go from the raw frames to a catalog with photometric, polarimetric and astrometric data in an efficient way is thus evident.

Over the years we have developed PCCDPACK (Pereyra 2000; Pereyra & Magalhães 2004), that provided one such reduction tools as an IRAF package. PCCDPACK is used at certain astronomy centers in Brazil, Chile, USA and elsewhere. SOUTH POL and its $\sim$2 deg^2 field presented an additional challenge and an even more automatic pipeline would be needed. This paper presents one such pipeline to address this need: SOLVEPOL. The main advantage of SOLVEPOL over the previous PCCDPACK routines is that the pipeline reduces the data fully automatically without user interaction – the previous reduction package is semiautomatic – , speeding up the reduction process.

This paper is organised as follows. The description of the data is presented in section 2. The description of the pipeline is given in section 3. Results of pilot studies on polarised standard stars, the field HD110984 and the Musca Dark Cloud, are presented in section 4. Finally, the conclusion is given in section 5.

2. Data acquisition

The polarimetric data that we have analyzed with this new pipeline was acquired in the optical with the Instituto de Astronomía, Geofísica e Ciências Atmosféricas polarimeter (IAGPOL) mounted on the 60-cm and 1.60-m telescopes at Observatório do Pico dos Dias (OPD) (Magalhães et al. 1996). IAGPOL consists of a half-wave plate that can be rotated in steps of 22.5°, a Savart calcite prism, and the CCD detector. For more details on the optical elements see Magalhães et al. (1996).

The Savart calcite is composed of two calcites cemented so that their principal axes are perpendicular to each other. The first calcite splits the incident beam of light into two components: the "ordinary" component that is propagated along the path of the incident beam, and the "extraordinary" component whom direction of propagation is deviated form the path of the incident beam. After the two rays traverse the first calcite and enter to the second calcite, the extraordinary ray becomes the ordinary ray, and the ordinary ray becomes the extraordinary ray. Therefore, a single image appears double on the CCD with the use of the Savart calcite. Figure 1 shows a typical image obtained when using the IAGPOL showing the star doublets. An advantage of the Savart calcite is that the astigmatism and color aberration are avoided compared with a single clacite, and that, because the ordinary and extraordinary images are perpendicularly polarized to each other, the polarization of the sky is cancelled out (eg., Hecht 2001), allowing observations under non-photometric conditions.

3. Description of the pipeline

SOLVEPOL is written in INTERACTIVE DATA LANGUAGE (IDL). It uses functions and proce-

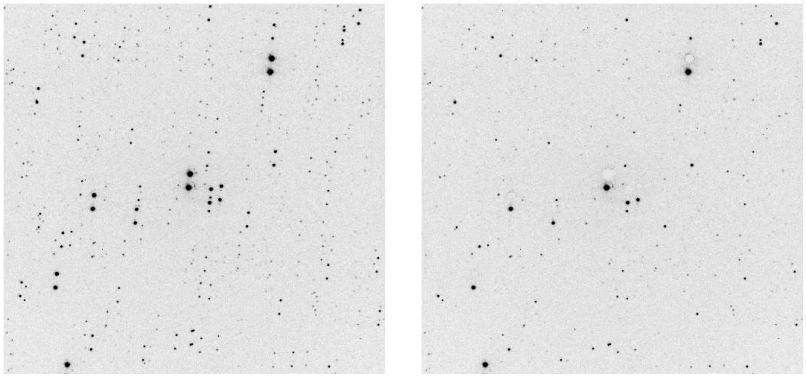

Fig. 1.— Observations with the polarimetric drawer (Magalhães et al. 1996) mounted on the 0.6-m telescope at OPD, Brazil. Left: Field centered on HD110984 (18×18 arcmin) showing a typical image with the doublet of each star (ordinary and extraordinary) produced by the Savart calcite. Right: Same field masked out by SOLVEPOL to calculate the astrometry (see section 3.3).

dures that are found in the IDL Astronomy Library (Landsman 1993) and in the Coyote Graphics Library[1]. It also makes use of ASTROMETRY.NET suite, a very useful software for astrometric purposes that is called by the pipeline.

SOLVEPOL corrects the raw images for bias and flats, and calculates the polarization (P), polarization angle (θ) and the visual magnitude (V) of the detected stars in the field. The main final product is a catalogue in plain text format which also contains the right ascension (RA) and declination (Dec) of all stars. The polarization signal-to-noise, P/σ_P, and the ratio F/σ_s, where F is the flux of a star and σ_s is the standard deviation from the median of the sky, are the only initial parameters to be set by the user and are used to reject weak sources.

In addition, we developed two procedures to analyse the data generated by SOVEPOL: MERGE and FILTER.

- MERGE merges two catalogues calculating the weighted mean of P, θ and V of the overlapped stars. MERGE reads the position, RA and Dec, of stars in two catalogues, and finds stars that match within a box with 0.001 degrees (3.6 arcsec) side. The stars that match position and those that don't match are printed into a third catalogue.

- FILTER constrains a catalogue, created by SOLVEPOL or MERGE, by setting lower and upper limits to the P, θ and V, and lower limits to P/σ_P and F/σ_s. These limits are set by the user in interactive mode for an ad hoc analysis. The output of FILTER is a subset of the original catalogue filtered by the chosen constraints.

3.1. Data reduction

The data reduction procedure that the pipeline applies is based on the standard procedure explained by Massey (1997). Roughly the procedure followed by the routine is as follows:

- First, the bias frames are median combined. Then, using the IDL SIGMA_FILTER procedure, sigma clipping is applied to remove pixels that deviate by more than 2.5 sigma from the median value of the neighboring 300 by 300 pixels. Finally, the overscan region is fit with a polynomial of order 2 and subtracted to create the master-bias frame.

[1] `http://www.idlcoyote.com/`

- For flat field frames, the overscan region is fit as described previously and is subtracted to each flat field frame. Next, the flat fields are median combined. Then, sigma clipping is applied as before, and the master-bias is subtracted to create the master-flat frame.

- Each source image is reduced by first fitting a polynomial of 2nd order to the overscan region, and subtracting this fit from the image. The master-bias is then subtracted and the result is then divided by the master-flat frame normalised to the median of the sky. Finally, the source images are trimmed to remove the overscan region.

If multiple images were observed per position angle of the waveplate, they are median combined after performing the reduction steps outlined before. The pipeline estimates and corrects for any possible shifts in X and Y between images before combining.

3.2. Polarization

The pipeline finds all sources and performs photometric measurements which are used to calculate their polarization. Aperture photometry is performed on both the ordinary and extraordinary images (F_o and F_e respectively) with ten concentric apertures ranging in size from 1 to 10 pixels in radius.

These apertures are based on the seeing measured in stars observed at OPD. Figure 2 shows the measured seeing in pixel units. The seeing ranges from 2 to 8 (1.3 arcsec to 5.2 arcsec), but we know that the seeing of stars out of focus due to cirrus is 7 to 8 (4.5 arcsec to 5.2 arcsec). Under good observational conditions at OPD, a seeing of ~ 3.5 pixels (2.3 arcsec) is expected. Thus, the 10 concentric apertures will cover all seeing conditions. For each aperture an annulus, with fixed inner and outer radii of 10 and 20 pixels respectively, is used to estimate the sky.

The polarimetry is measured using the same aperture for all waveplate positions, and the size aperture that gives the lowest error in the polarimetry is selected to calculate the final polarimetric properties of a star.

The modulation of the intensity, z_i, where i is the position number of the half-wave plate, is estimated as follows

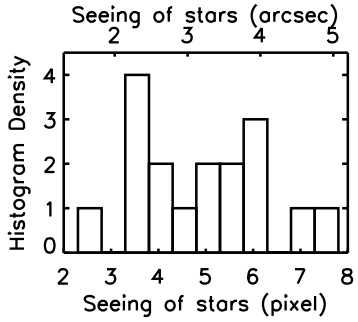

Fig. 2.— Seeing of stars observed with the telescopes of the OPD/LNA in pixel units. The seeing ranges from 2 to 8, thus the 10 concentric apertures to perform the polarimetric measurements is justified.

$$z_i = \frac{F_{e,i} - F_{o,i}(F_e^T/F_o^T)}{F_{e,i} + F_{o,i}(F_e^T/F_o^T)}, \quad (1)$$

where $F_{o,i}$ and $F_{e,i}$ are the fluxes of the ordinary and extraordinary images at the position i of the waveplate, and F_o^T and F_e^T are the ordinary and extraordinary total flux of a star summed on all the waveplate's positions, respectively (see Magalhães et al. 1984). The stokes parameters Q and U for each source are then calculated as follows.

$$Q = \frac{2}{\mu}\sum_i^{\mu} z_i cos(4\psi_i) \quad (2)$$

$$U = \frac{2}{\mu}\sum_i^{\mu} z_i sin(4\psi_i) \quad (3)$$

where μ is the number of positions of the half-wave plate and $\psi_i = 0°, 22.5°, 45°, 67.5°$, etc. This yields the percent linear polarization, P, and the polarization angle, θ, measured from north to east after the zero-angle is calibrated using standard stars.

$$P = \sqrt{Q^2 + U^2} \quad (4)$$

$$\theta = \frac{1}{2} tan^{-1}\frac{U}{Q} \quad (5)$$

The modulation of the intensity of each star is fit and the reduced χ^2 calculated. For this work, those stars with $\chi^2 > 6.0$ are rejected. This limit was set by empirical grounds. Figure 3 shows the χ^2 of the stars of the Musca field analysed in this

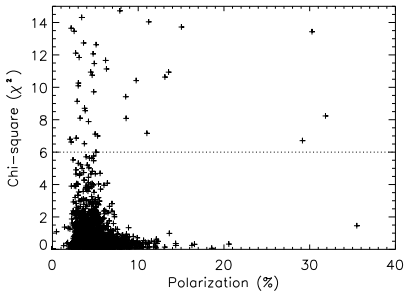

Fig. 3.— Chi square (χ^2) of the modulation fit vs Polarization of the stars in Musca fields analyzed in this work. $\chi^2 > 6$ is a reasonable limit to reject stars with bad modulation fit and therefore spurious polarization. $F/\sigma_s \geq 5.0$ and $P/\sigma_P \geq 5$.

work (in section 4). As it can be seen, a $\chi^2 = 6.0$ separates reasonable good those stars belonging to the Musca cloud and those showing unexpected high polarization. Therefore, a $\chi^2 \leq 6.0$ would include a reasonable sample with real polarization. This test was applied in other fields with same result. However, a different cut of χ^2 can be selected by the user of SOLVEPOL.

3.3. Astrometry calibration

SOLVEPOL uses the ASTROMETRY.NET software[2] to calibrate the astrometry of an image and get the accurate celestial coordinates of the stars. The pipeline masks out one of the components of the doublet of each star emerging from the Savart calcite on the first waveplate position's image, to get a 'normal' image of the sky. Figure 1 shows the original image from the first waveplate position (left), and after applying the mask (right). In this case the component to the right and up have been masked out for each star. The masked regions are replaced with the mean sky value of the image. This 'normal' image is processed by the ASTROMETRY.NET software[3].

[2]ASTROMETRY.NET is a project partially supported by the US National Science Foundation, the US National Aeronautics and Space Administration, and the Canadian National Science and Engineering Research Council. For more information go to `http://astrometry.net`.

[3]Alternatively, in the case that the astronomy.net software is not installed in the running computer, a list of positions of the detected stars sorted by brightness is produced to be used directly in the web version of ASTROMETRY.NET.

The ASTROMETRY.NET software finds, in the masked image, the relative positions of nearby groupings of 3 or 4 stars on the field, and finds their corresponding triples or quadruplets in the 2MASS and Tycho-2 catalogues. Each grouping generates a candidate matching sky, and ASTROMETRY.NET finds the true matching view. After an alignment of the image and the catalogues, ASTROMETRY.NET gives the astrometric solution that the pipeline includes in the masked image header. This image/information is then used for coordinates to translate from pixels to RA and Dec of the detected sources.

3.4. Photometry and magnitude calibration

New photometric measurements are applied to both the ordinary and extraordinary images within an aperture with diameter 2 times the average full width at half maximum (FWHM) of the brightest stars in the field. The FWHM is estimated in the first waveplate position's image. If the FWHM is greater than 10 pixels, an aperture of 10 pixels in radius is used. We define the measured flux, F_m, as the sum of the ordinary and extraordinary fluxes. For our observations taken in the V-band, the pipeline obtains the visual magnitude:

$$V = m_z - 2.5log(F_m) \quad (6)$$

where m_z is the zero point magnitude calibrated with the Guide Star Catalog version 2.3 (GSC v2.3. Lasker et al. 2008). This catalogue goes down to 18th magnitude[4]. The position in RA and Dec are used to match the stars. We define m_z as the mean of the absolute difference (to avoid that the sum is zero) between our measured magnitude, $m_{\rm mea,i}$, and the optical magnitude reported in the GSC v2.3, $m_{{\rm cat},i}$, for at most the 25 brightest stars in the field, i.e., $m_z = \frac{1}{k}\sum_{i=1}^{k} | m_{{\rm mea},i} - m_{{\rm cat},i} |$, where k is at most 25. If there are no stars with measured magnitude in the field, m_z is set to 0 (no calibration).

[4]The pipeline code can be modified to calibrate with any catalogue available in the VizieR database over the web.

4. Results

We conducted pilot studies to test our new pipeline SOLVEPOL. These include the analysis of ten standard stars (essential for calibration), the field centred on HD110984 (a well studied field in our group), and the already published 1997 observational campaign on Musca (Pereyra & Magalhães 2004, hereafter PM04). We fixed $F/\sigma_s \geq 5.0$ for this present work – a limit for a confident source detection.

4.1. Standard stars

The analysis of polarized standard stars is essential to check the veracity of our results. For the 10 standard stars shown in Table 1, we preset polarization and magnitude results using SOLVEPOL and compare these with reported values from the literature. The standard stars were observed during different observational campaigs, most of them in the 1997 Musca's campaign (PM04).

Although the standard stars are used to get the zero-angle calibration of the observations, the disposition of the telescope relative to the sky or to different positions of the waveplate inside the polarimeter is not the same between observing campaings. Hereby, the angle θ is meaningless to compare between stars observed in different campaings, and it is not tabulated in Table 1. The position of HD100623, HD147084 and HD154445 could not be solved because less than three stars fall in their field – at least three stars are needed to solve the astrometry – therefore, its RA and Dec are not tabulated for its comparison with the literature.

Figure 4, shows plots comparing P and V of the standard stars calculated with SOLVEPOL compared to values from the literature. These results are consistent to well within 2σ. The P that deviate by more corresponds to HD147084: our P is lower than the reported in Turnshek et al. (1990) by a factor of 0.9. However, P still matches within the error bars. On the other hand, the V that deviate by more corresponds to HD298383: our V is higher than the reported in Turnshek et al. (1990), by a factor of 1.1 (see Table 1). Because we do not see in Figure 4 a systematic displacement from the line representing the equality, the discrepancy in V-band magnitude can be attributed to climatological differences along the observation (clouds, cirrus, etc.).

4.2. HD110984 and its field

We have analysed the field around HD110984. Figure 5 shows the distributions of P, θ and V, and P versus V for the HD110984 field measured with SOLVEPOL and the PCCDPACK routines for comparison. We fixed $F/\sigma_s \geq 5.0$ and $P/\sigma_P \geq 5$ for this analysis.

The distributions produced by both routines are quite similar. In particular, the distributions of polarization and position angle indicate that both routines will lead to the same conclusion about the polarimetric properties on the field of HD110984. An aspect to note is that there are stars detected by SOLVEPOL, but were not detected by the PCCDPACK routines (and vice versa). This can be clearly seen in Figure 6, which shows the polarization maps of the field centred on HD110984.

In Figure 7 we compare the number of sources detected by SOLVEPOL and PCCDPACK. The number of sources detect by SOLVEPOL is higher than the number of sources detected by the PCCDPACK routines for low values of P/σ_P (with $F/\sigma_s \geq 5.0$). Therefore, our new pipeline seems to be producing more complete catalogues. However, the number of sources detected by both routines tends to converge towards greater values of P/σ_P. For instance, for $P/\sigma_P = 3$, the number of stars detected by SOLVEPOL is 154, and the number of sources detect by the PCCDPACK routines is 134 – a difference of 20 detected stars –, while for $P/\sigma_P = 5$ (an usual ratio for a confident measurement) the difference is just 6 stars (101 and 95 detection by SOLVEPOL and the PCCDPACK routines, respectively).

Finally, in Figure 8 we compare P, uncertainty in the polarization (σ_P), θ and V using SOLVEPOL versus those using the PCCDPACK routines. For the same stars found by SOLVEPOL and the PCCDPACK routines, it can be see that both routines produce consistent results with each other to within 3σ. Therefore, both routines give results that will lead to the same conclusions when analysing the same field.

Table 1: Standard stars analysed. Our measurements and those from the literature (last line for each star) are shown. RA, Dec and V are from the GSC v2.3 catalogue (Lasker et al. 2008); P is from: (a) (Bastien et al. 1988), (b) (Serkowski et al. 1975) and (c) (Turnshek et al. 1990). '—' indicates that the position could not be obtained by the pipeline because of the lack of reference stars on the filed (see Section 4.1 for details).

Star	RA J2000	Dec J2000	V (mag)	P (%)	Obs. date	Ref.
HD80558	09 18 42.44	−51 33 37.69	5.29 ± 0.20	3.25 ± 0.02	1997-04-09	...
	09 18 42.36	−51 33 38.34	5.94 ± 0.01	3.11 ± 0.01	...	a
HD84810	—	—	—	1.67 ± 0.07	1997-04-09	...
	09 45 14.81	−62 30 28.44	3.69 ± 0.03	1.58 ± 0.01	...	a
HD100623	—	—	—	0.04 ± 0.06	1997-04-10	...
	11 34 29.49	−32 49 52.81	6.05 ± 0.01	$0.02\pm$*	...	b
HD110984	12 46 44.84	−61 11 11.91	9.19 ± 0.18	5.64 ± 0.05	2001-03-02	...
	12 46 44.84	−61 11 11.47	8.49 ± 0.16	5.79 ± 0.04	1997-04-12	...
	12 46 44.82	−61 11 11.47	8.55 ± 0.16	5.86 ± 0.03	1997-04-13	...
	12 46 44.84	−61 11 11.58	9.04 ± 0.02	5.70 ± 0.01	...	c
HD111613	12 51 18.05	−60 19 47.79	5.40 ± 0.18	3.20 ± 0.02	1997-04-09	...
	12 51 17.98	−60 19 47.24	5.77 ± 0.01	3.06 ± 0.01	...	a
HD126593	14 28 50.87	−60 32 24.94	8.60 ± 0.29	4.94 ± 0.06	2001-03-02	...
	14 28 50.87	−60 32 25.12	8.70 ± 0.01	5.02 ± 0.01	...	c
HD147084	—	—	—	3.79 ± 0.35	1997-04-10	...
	16 20 38.18	−24 10 09.55	4.66 ± 0.01	4.17 ± 0.01	...	c
HD154445	—	—	—	3.79 ± 0.05	1997-04-10	...
	17 05 32.26	−00 53 31.44	5.65 ± 0.01	3.80 ± 0.08	...	c
HD155197	17 10 15.74	−04 50 03.62	9.60 ± 0.09	4.56 ± 0.04	1997-04-12	...
	17 10 15.75	−04 50 03.67	9.57 ± 0.03	4.63 ± 0.02	...	c
HD298383	09 22 29.77	−52 28 57.65	10.78 ± 0.72	5.17 ± 0.06	2001-03-01	...
	09 22 29.77	−52 28 57.36	10.74 ± 0.37	5.43 ± 0.04	1997-04-13	...
	09 22 29.76	−52 28 57.25	10.78 ± 0.34	5.38 ± 0.06	1997-04-12	...
	09 22 29.77	−52 28 57.25	9.75 ± 0.03	5.23 ± 0.01	...	c

* error not given in reference b.

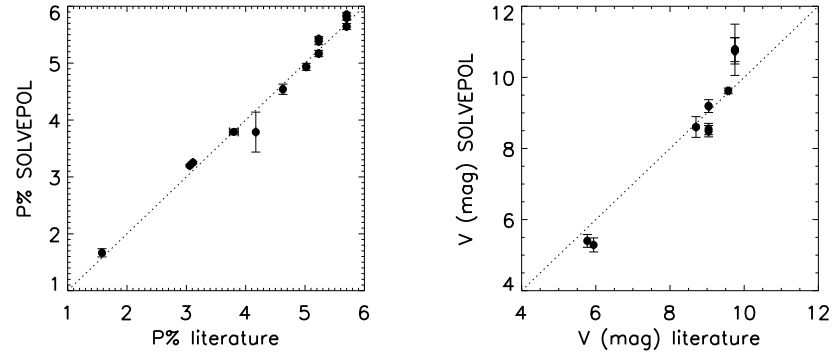

Fig. 4.— Left: Polarization of the standard stars reduced with SOLVEPOL versus the polarization in the literature (see Table 1). Right: V magnitudes reduced by SOLVEPOL versus the V magnitude from the GSC catalogue version 2.3. Dashed line represents the equality. The polarization and optical magnitudes are consistent within less than 2σ. The ploted error bars are 1σ.

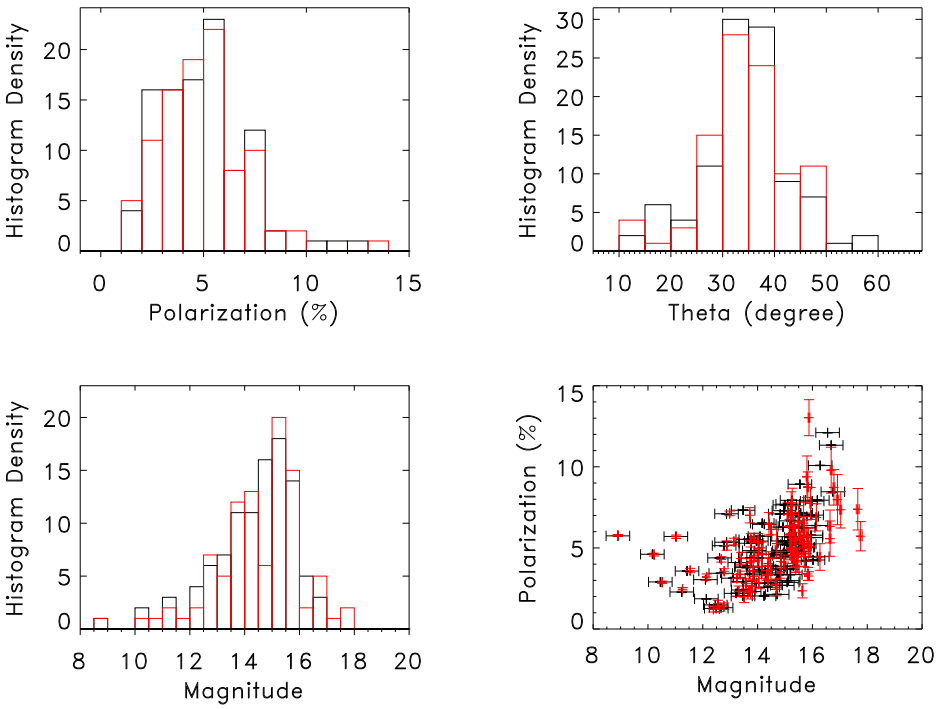

Fig. 5.— Distributions of P, θ and V, and P versus V measured by SOLVEPOL (black) and the PCCDPACK routines (red) of the field centered on HD110984. These distributions correspond to $F/\sigma_s \geq 5.0$ and $P/\sigma_P \geq 5$.

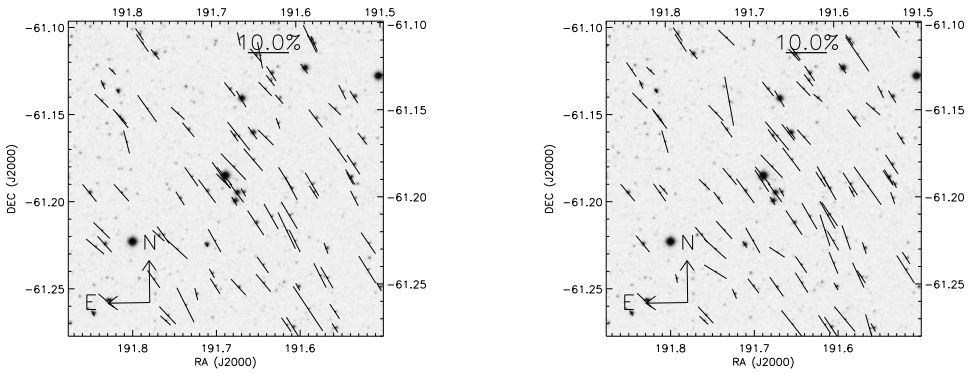

Fig. 6.— Left: Polarization map of the field centred on the standard star HD110984 reduced with the PCCDPACK routines. Right: Same field reduced with SOLVEPOL. $F/\sigma_s \geq 5.0$ and $P/\sigma_P \geq 5$. Note that the polarization vectors result of our new pipeline are consistent with those obtained by the previous routines. Few stars in the left figure are not present in the right figure and vice versa, indicating a subtle difference in the source detection procedure.

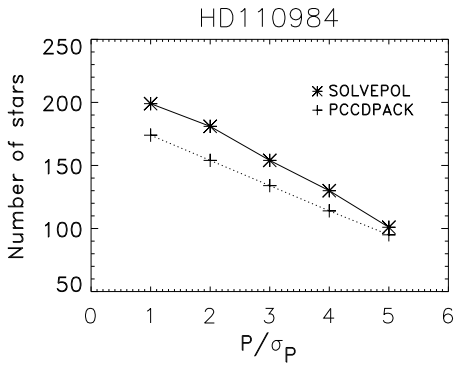

Fig. 7.— Number of detected stars on the field of HD110984 versus P/σ_P measured by SOLVEPOL (asterisk signs) and by PCCDPACK routines (plus signs). F/σ_s is fixed to ≥ 5.0. Dot and solid lines are simply joining the points. Notice that the number of sources converge towards greater values of P/σ_P. For instance for $P/\sigma_P \geq 5$ the difference in number of detected stars is only 6.

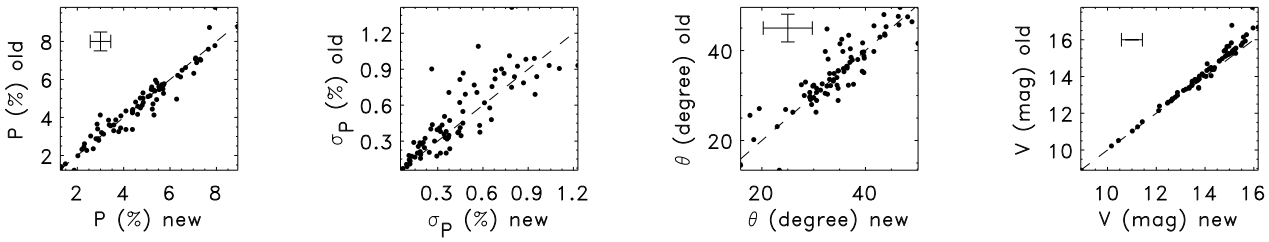

Fig. 8.— From left to right: P, σ_P, θ and V measured with SOLVEPOL (new) and those measured by the previous PCCDPACK routines (old) on HD110984's field. Dashed line represents the equality. The mean 1σ error bar is indicated.

4.3. Musca Dark Cloud data

A comparison of our results with those reported in PM04 of the well studied field of the Musca Dark Cloud is presented in this section. We analyze all the fields observed in the 1997 campaign. The observational details are described in PM04. The source detection limits used in SOLVEPOL were set to $F/\sigma_F \geq 5.0$ and $P/\sigma_P \geq 5.0$, same limits adopted by PM04, but using the PCCDPACK routines.

In Figure 9 the polarization P, uncertainty in the polarization (σ_P), θ and V calculated by SOLVEPOL, and those from the catalogue of PM04 are presented. As it can be seen, P, σ_P, θ and V are all consistent with each other, with some degree of scattering within 3σ. The catalogues produced by SOLVEPOL were processed with MERGE, therefore, there are no repeated stars from the overlapping field regions. On the other hand, the catalogue (reported in VizieR) of PM04 includes two entries for stars in overlapping regions, increasing the total number of results. The uncertainty in V is not reported by PM04, and thus we cannot compare our uncertainties against theirs.

The distributions of P, θ, and V for Musca are shown in Figure 10. The sample reduced with SOLVEPOL seems to be complete in magnitude up to 17 mag. This is 1.5 magnitudes deeper than the 15.5 mag reported in PM04 using PCCDPACK.

Table 2 shows the field numbers (we have adopted the same notation used in PM04), its central position calculated by our pipeline, the number of detected stars, and the median of P, θ and V with their respective uncertainties (standard deviation from the mean) and those from PM04 for comparison. We adopted the limit of $P/\sigma_P \geq 10.0$, same as in the table reported by PM04, their table 5, for a direct comparison.

The total number of stars with $P/\sigma_P \geq 10.0$ is 859, slightly higher than the 846 sources reported by PM04. About individual fields, the greatest difference in the number of detected stars is 9 (SOLVEPOL found more) which correspond to field number 24 (see Table 2). However, as it can be seen in Figure 11 (left figure), that compares the number of sources vs P/σ_P (F/σ_F fix to 5) detected by SOLVEPOL and the PCCDPACK routines, the number of sources detected by both routines tend to converge for high values of P/σ_P.

Overall, mean values of P, θ and V, tabulated in Table 2, and plotted in Figure 11 for an easier inspection, are consistent with the mean values of P, θ and V reported by PM04, their table 5, reproduced here in Table 2.

Figure 12 shows the polarization maps on the Musca region of the fields analysed in this work and tabulated in Table 2 calculated by SOLVEPOL. Each vector represents one object. Again, our polarization maps and those reported by PM04 are consistent.

5. Conclusions

We have described a new pipeline for reducing imaging polarimetry data: SOLVEPOL. From the raw images, it produces a catalog of the observed field with photometric, polarimetric and astrometric information. We have compared results from SOLVEPOL with those from PCCDPACK and found them to be consistent. There is a tendency for SOLVEPOL to produce more complete catalogs possibly due to rounding errors and small differences in the codes.

As it stands, SOLVEPOL is directly applicable to images obtained with birefringent polarizers, such as the simple calcite plate and the Savart plate. It should not be difficult to addapt it to single-image polarizers, such as dichroic polarizers. Another work in progress is adapting the pipeline to NIR imaging polarimetry. The current version of SOLVEPOL will be made available as a free download at `http://www.astro.iag.usp.br/~ramirez/pipeline.html`. It is hoped that the optical/IR polarimetry community can contribute to its continuous improvement.

EAR acknowledges FAPESP grant (2012/00185-8). AMM acknowledges support for his group's activities at IAG from the agencies FAPESP (grant no. 2010/19694-4), CNPq and CAPES. JWD acknowledges funding from the Brazil-U.S. Physics Ph.D. Student & Post-doc Visitation Program sponsored by the Sociedade Brasileira de Fsica and the American Physical Society. This research has made use of the VizieR catalogue access tool, CDS, Strasbourg, France. The original description of the VizieR service was published in A&AS 143, 23.

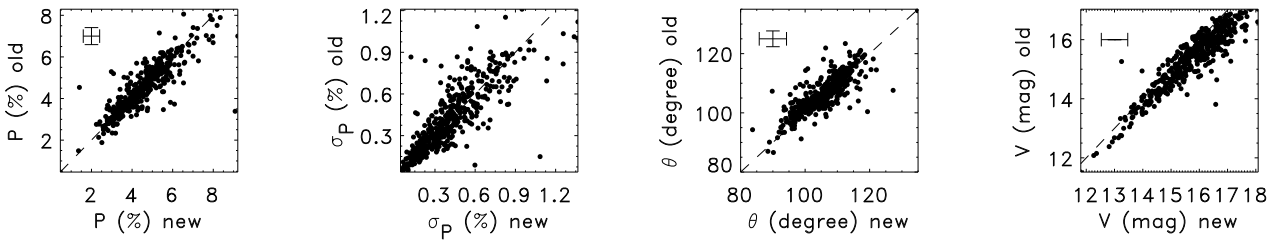

Fig. 9.— From left to right: P, σ_P, θ and V measured with SOLVEPOL (new) and those reported in VizieR obtained by PM04 using the PCCDPACK routines (old). $F/\sigma_s \geq 5.0$ and $P/\sigma_P \geq 5$. Dashed line represents the equality. The mean 1σ error bar is indicated. Our results are consistent with those reported of PM04 within 3σ.

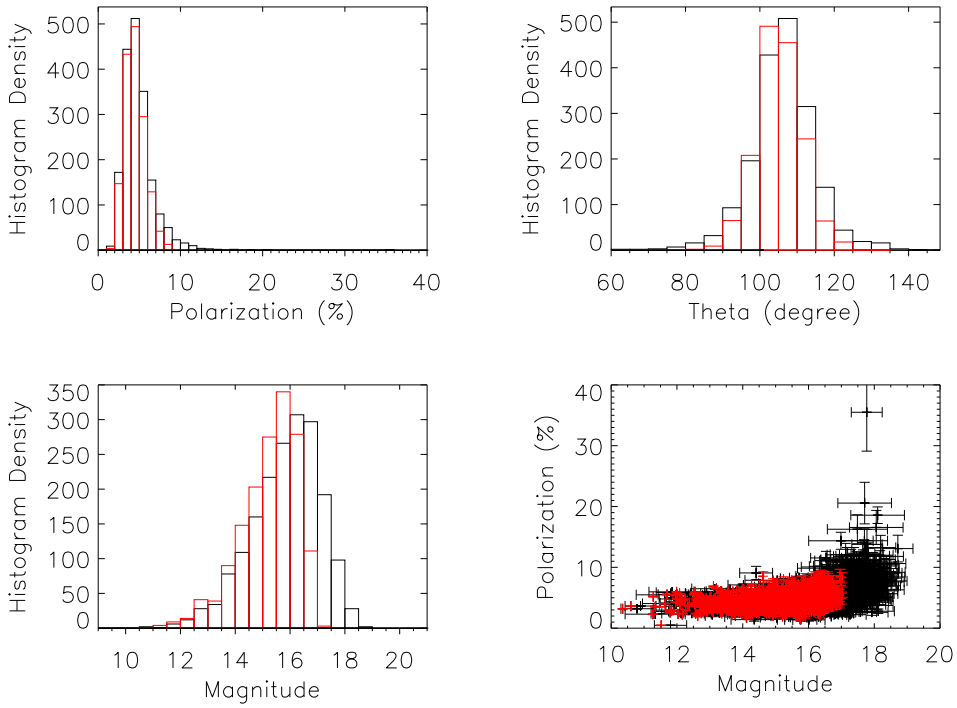

Fig. 10.— Distributions of P, θ, V, and P versus V of Musca measured by SOLVEPOL (black) and by the PCCDPACK (red). $F/\sigma \geq 5.0$ and $P/\sigma_P \geq 5.0$.

Table 2: Fields of Musca reduced by SOLVEPOL using the values $P/\sigma_P \geq 10.0$ and $F/\sigma \geq 5.0$. Median of P, θ and V and its standard deviation from the mean. Below the lane, same fields of Musca but reported by PM04 and using the same P/σ_P and F/σ limits.

Field	RA J2000	Dec J2000	N	median P	median θ	median V
	Central Region			(%)	(°)	(mag)
03	12 35 05.73	−71 00 30.80	61	3.22 ± 1.26	102.23 ± 13.51	15.46 ± 1.22
05	12 30 06.91	−71 00 35.20	48	3.95 ± 0.92	105.73 ± 4.03	15.50 ± 1.07
08	12 27 36.99	−71 08 40.13	46	3.70 ± 0.77	108.23 ± 4.17	15.00 ± 1.12
11	12 30 10.15	−71 24 38.34	35	4.34 ± 0.90	105.93 ± 5.25	15.50 ± 1.29
13	12 25 13.27	−71 24 40.64	64	5.17 ± 0.80	110.63 ± 3.09	15.47 ± 1.07
14	12 27 43.58	−71 32 35.64	33	5.21 ± 1.55	106.16 ± 8.44	15.63 ± 1.14
16	12 27 50.15	−71 41 00.17	61	4.92 ± 0.86	99.521 ± 4.94	15.73 ± 1.19
20	12 25 12.13	−72 00 56.48	67	4.80 ± 1.05	107.60 ± 4.50	15.30 ± 1.18
22	12 25 18.97	−72 09 19.19	63	4.12 ± 2.24	110.20 ± 8.11	14.92 ± 1.16
24	12 19 58.77	−72 09 33.49	87	4.70 ± 1.05	104.70 ± 3.90	14.91 ± 1.18
26	12 20 06.32	−72 17 26.06	75	5.04 ± 1.76	105.73 ± 4.03	14.86 ± 1.08
27	12 22 33.51	−72 25 16.68	41	5.33 ± 1.37	115.50 ± 14.94	14.89 ± 1.00
29	12 19 57.42	−72 33 32.76	53	4.81 ± 1.50	102.12 ± 5.64	15.10 ± 1.40
30	12 18 02.47	−72 33 39.58	71	3.30 ± 0.94	110.15 ± 3.70	14.41 ± 1.13
34	12 37 56.59	−70 41 10.27	54	3.04 ± 1.16	104.95 ± 5.00	14.42 ± 1.20
03	12 35 27.35	−71 00 31.29	55	3.15 ± 0.02	102.31 ± 1.79	15.45 ± 1.00
05	12 30 28.02	−71 00 34.25	54	3.80 ± 0.02	106.17 ± 1.62	15.47 ± 1.01
08	12 27 58.53	−71 08 35.56	48	3.52 ± 0.03	107.38 ± 1.97	15.50 ± 1.06
11	12 30 28.59	−71 24 34.25	34	3.88 ± 0.03	105.95 ± 1.55	15.34 ± 1.11
13	12 25 29.15	−71 24 36.75	65	4.93 ± 0.02	111.53 ± 1.53	15.43 ± 0.97
14	12 27 59.05	−71 32 35.56	34	5.01 ± 0.03	106.96 ± 1.67	15.37 ± 1.10
16	12 27 59.23	−71 40 35.56	62	4.67 ± 0.03	102.71 ± 1.70	15.47 ± 0.97
20	12 05 29.89	−72 00 36.75	64	4.56 ± 0.03	105.13 ± 1.71	15.42 ± 0.98
22	12 25 30.06	−72 08 36.75	65	3.92 ± 0.02	107.74 ± 1.76	15.43 ± 0.97
24	12 20 15.82	−72 08 38.87	78	4.70 ± 0.02	102.45 ± 1.57	15.48 ± 1.00
26	12 20 15.95	−72 16 38.87	68	5.03 ± 0.02	101.81 ± 1.60	15.44 ± 1.00
27	12 22 53.25	−72 24 37.87	49	5.17 ± 0.03	113.36 ± 1.65	15.48 ± 1.05
29	12 20 16.23	−72 32 38.87	52	4.51 ± 0.02	99.72 ± 1.70	15.50 ± 1.03
30	12 17 39.05	−72 32 39.74	69	3.25 ± 0.02	107.20 ± 1.64	15.45 ± 1.00
34	12 38 03.74	−70 40 29.55	49	2.67 ± 0.02	104.24 ± 1.74	15.48 ± 1.05

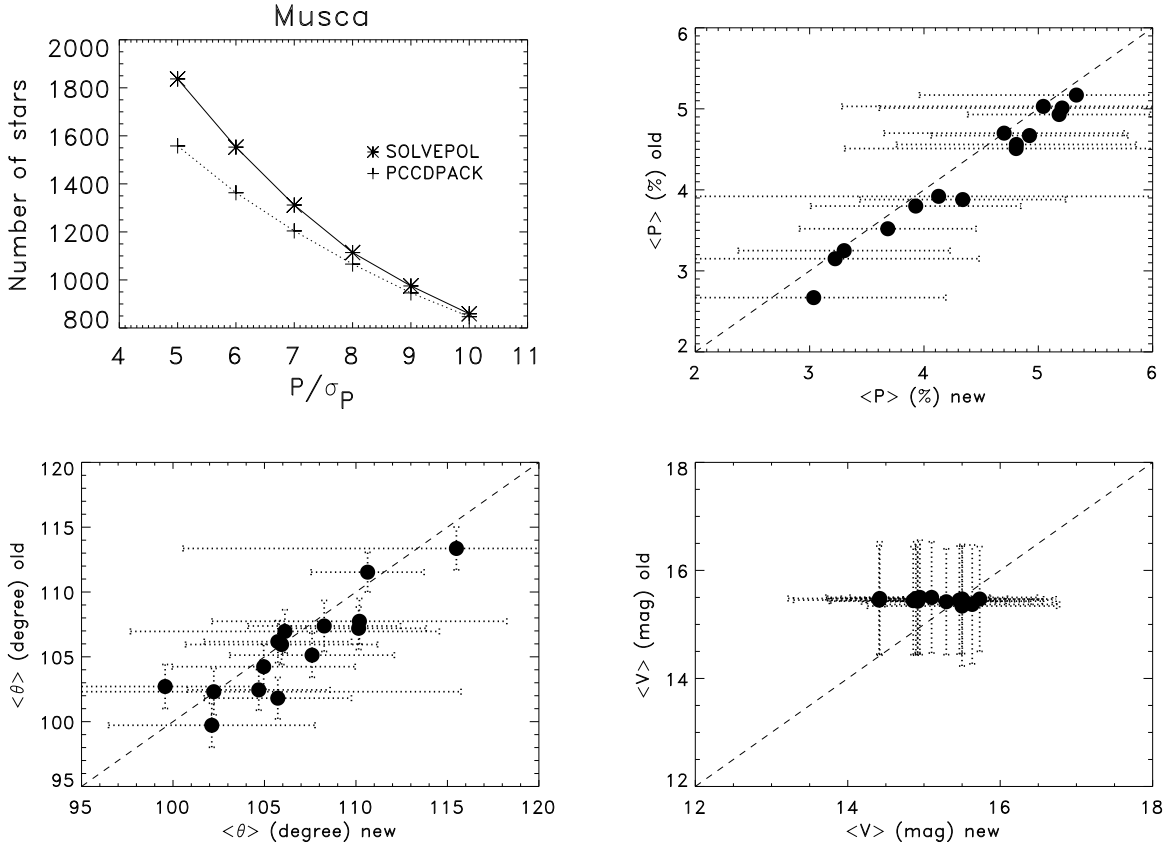

Fig. 11.— Top Left: number of detected stars of Musca versus P/σ_P measured with SOLVEPOL (asterisk signs) and the number of sources reported in VizieR obtained by PM04 using the PCCDPACK routines (plus signs). F/σ_s is fixed to ≥ 5.0. Clearly the number of sources converge towards greater values of P/σ_P. Top Right: mean values of P measured with SOLVEPOL (new) and mean values of P reported in VizieR obtained by PM04 (old). Bottom Left: mean values of θ measured with SOLVEPOL (new) and mean values of θ reported in VizieR obtained by PM04 (old). Bottom Right: mean values of V measured with SOLVEPOL (new) and mean values of V reported in VizieR obtained by PM04 (old). The error bars are our calculated standard deviation from the mean, except for $< P >$ and $< \theta >$ reported by PM04, which we took directly from their table. The data of these plots are also reproduced in Table 2.

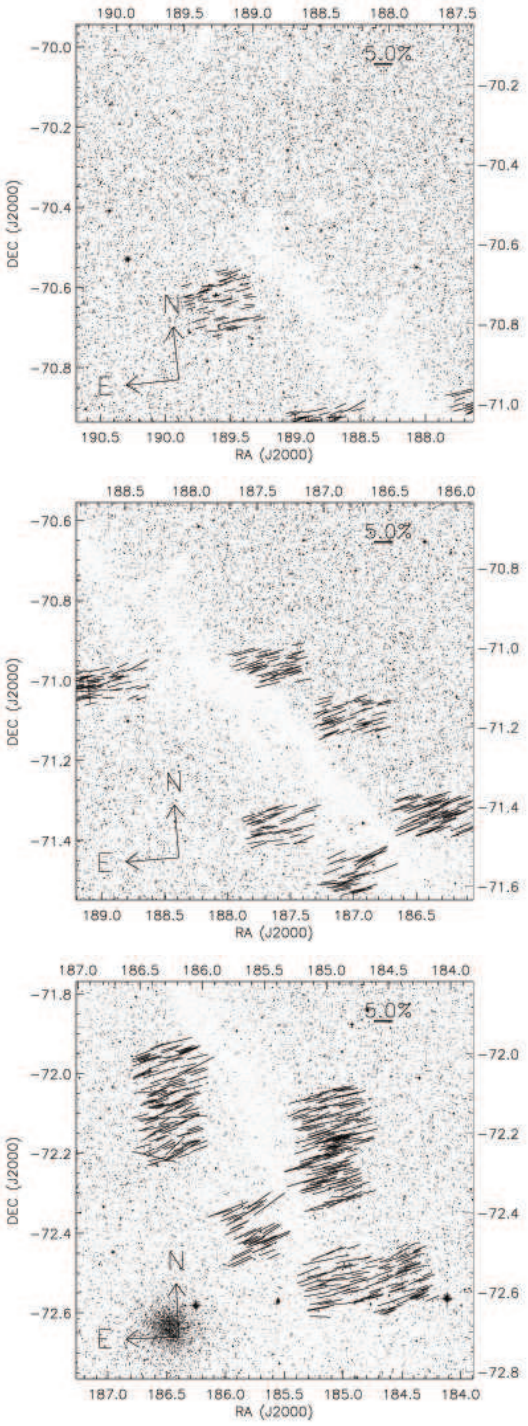

Fig. 12.— Polarization maps of Musca produced with SOLVEPOL. $F/\sigma \geq 5.0$ and $P/\sigma_P \geq 10$. These results are consistent with those reported in PM04.

REFERENCES

Adamson, A., Aspin, C., Davis, C., & Fujiyoshi, T., eds. 2005, Astronomical Society of the Pacific Conference Series, Vol. 343, Astronomical Polarimetry: Current Status and Future Directions

Bastien, P., Drissen, L., Menard, F., Moffat, A. F. J., Robert, C., & St-Louis, N. 1988, AJ, 95, 900

Bastien, P., Manset, N., Clemens, D. P., & St-Louis, N., eds. 2011, Astronomical Society of the Pacific Conference Series, Vol. 449, Astronomical Polarimetry 2008: Science from Small to Large Telescopes

Clemens, D. P., Pinnick, A. F., Pavel, M. D., & Taylor, B. W. 2012, ApJS, 200, 19

Hecht, E. 2001, Optics 4th edition (Addison-Wesley Publishing Company)

Landsman, W. B. 1993, in Astronomical Society of the Pacific Conference Series, Vol. 52, Astronomical Data Analysis Software and Systems II, ed. R. J. Hanisch, R. J. V. Brissenden, & J. Barnes, 246

Lasker, B. M., Lattanzi, M. G., McLean, B. J., Bucciarelli, B., Drimmel, R., Garcia, J., Greene, G., Guglielmetti, F., Hanley, C., Hawkins, G., Laidler, V. G., Loomis, C., Meakes, M., Mignani, R., Morbidelli, R., Morrison, J., Pannunzio, R., Rosenberg, A., Sarasso, M., Smart, R. L., Spagna, A., Sturch, C. R., Volpicelli, A., White, R. L., Wolfe, D., & Zacchei, A. 2008, AJ, 136, 735

Magalhães, A. M., Benedetti, E., & Roland, E. H. 1984, PASP, 96, 383

Magalhães, A. M., de Oliveira, C. M., Carciofi, A., Costa, R., Dal Pino, E. M. G., Diaz, M., Ferrari, T., Fernandez, C., Gomes, A. L., Marrara, L., Pereyrac, A., Ribeiro, N. L., Rodrigues, C. V., Rubinho, M. S., Seriacopi, D. B., & Taylor, K. 2012, in American Institute of Physics Conference Series, Vol. 1429, American Institute of Physics Conference Series, ed. J. L. Hoffman, J. Bjorkman, & B. Whitney, 244–247

Magalhães, A. M., Pereyra, A., Melgarejo, R., de Matos, L., Carciofi, A. C., Benedito, F. F. C., Valentim, R., Vidotto, A. A., da Silva, F. N., de Souza, P. P. F., Faria, H., & Gabriel, V. S. 2005, in Astronomical Society of the Pacific Conference Series, Vol. 343, Astronomical Polarimetry: Current Status and Future Directions, ed. A. Adamson, C. Aspin, C. Davis, & T. Fujiyoshi, 305

Magalhães, A. M., Rodrigues, C. V., Margoniner, V. E., Pereyra, A., & Heathcote, S. 1996, in Astronomical Society of the Pacific Conference Series, Vol. 97, Polarimetry of the Interstellar Medium, ed. W. G. Roberge & D. C. B. Whittet, 118

Massey, P. 1997, A User's Guide to CCD Reductions with IRAF (http://iraf.noao.edu/docs/recommend.html)

Pereyra, A. 2000, PhD thesis, Depto. de Astronomia, Instituto Astronômico e Geofísico, USP, Rua do Matão 1226 - Cidade Universitária 05508-900 São Paulo SP - BRAZIL

Pereyra, A. & Magalhães, A. M. 2004, ApJ, 603, 584

Serkowski, K., Mathewson, D. S., & Ford, V. L. 1975, ApJ, 196, 261

Trujillo-Bueno, J., Moreno-Insertis, F., & Sanchez Martinez, F. 2002, Astrophysical Spectropolarimetry (Cambridge University Press)

Turnshek, D. A., Bohlin, R. C., Williamson, II, R. L., Lupie, O. L., Koornneef, J., & Morgan, D. H. 1990, AJ, 99, 1243

This 2-column preprint was prepared with the AAS LaTeX macros v5.2.